ACS Energy LETTERS

pubs.acs.org/journal/aelccp

Letter

Environmental Control of Tin Perovskite Crystallization via Solvent Vapor Fuming

Che-Hsin Kuo,‡ Yun-Sheng Shih,‡ Chun-Hsiao Kuan,‡ Shi-Jie Shen, Yi-Hao Wu, Hsin-Yu Hu, Han-Jung Li, Chieh-Ting Lin, and Eric Wei-Guang Diau*

Cite This: *ACS Energy Lett.* 2026, 11, 5211−5217

Read Online

ACCESS | Metrics & More | Article Recommendations | Supporting Information

ABSTRACT: We systematically explored solvent vapor treatment (SVT) using 12 different solvents to optimize lead-free tin perovskite solar cells (TPSCs) prepared via a two-step fabrication. Guided by density functional theory (DFT) and macroscopic parameter screening, 1,1,3,3-tetramethylurea (TMU) was identified as the superior fuming agent due to its high donor number, moderate dielectric constant (ε = 24.5), and optimal vapor pressure (∼1.6 Torr). These properties facilitate a controlled dissolution-recrystallization process, resulting in dense, strain-relaxed films with large grains, a low surface roughness with RMS 17.0 nm, and uniform surface potential. Advanced optoelectronic characterizations, including QFLS mapping and transient photovoltage/photocurrent (TPV/TPC) measurements, confirm that TMU treatment resolves the fundamental carrier dynamic trade-off—simultaneously enabling swift charge extraction (0.67 μs) and profoundly suppressing interfacial non-radiative recombination (75.14 μs). Consequently, the optimized TPSC achieved a record power conversion efficiency (PCE) of 10.45% alongside a maximized thermodynamic potential (QFLS peaking at 1.028 eV). Furthermore, the devices demonstrate exceptional long-term durability, exceeding 6000 hours of operational stability. This study highlights the critical role of multidimensional solvent engineering—bridging molecular interactions with macroscopic crystallization—to realize highly efficient and stable tin perovskite photovoltaics.

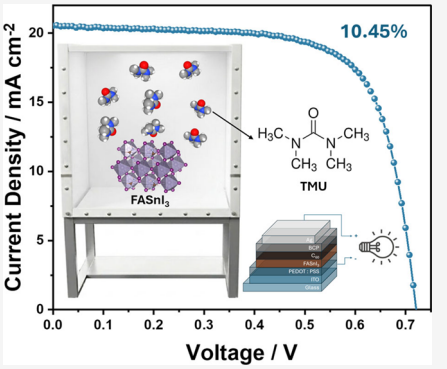

Tin-based perovskite solar cells (TPSCs) have emerged as a promising lead-free alternative to lead-based analogs.[1] However, the uncontrollable, rapid crystallization and inherent chemical instability of Sn^{2+} remain significant hurdles, often leading to poor film morphology, severe residual lattice strain and high trap densities.[2,3] Such microstructural defects not only aggravate non-radiative recombination but also accelerate the detrimental oxidation of Sn^{2+} to Sn^{4+}, causing severe p-type self-doping. Therefore, regulating the crystallization kinetics to achieve dense, pinhole-free, strain-free films is imperative. Solvent vapor treatment (SVT) has been recognized as a powerful post-treatment to modulate crystal growth via Lewis acid-base interactions, yet a systematic understanding of how specific solvent properties dictate these interactions remains elusive.[4]

In this work, we systematically screened twelve solvents with diverse physicochemical properties to optimize the performance of FA-based TPSCs prepared via a two-step method.[5] Guided by density functional theory (DFT), we identified 1,1,3,3-tetramethylurea (TMU) as the ultimate fuming agent, possessing a significantly stronger and more robust coordination affinity than DMSO. To comprehensively elucidate the superiority of TMU, we employed a suite of advanced characterization techniques. Grazing-incidence wide-angle X-ray scattering (GIWAXS) unveils that TMU successfully relieves macroscopic lattice strain, while photoluminescence-based quasi-Fermi level splitting (QFLS) mapping visually confirms a profound, homogeneous macroscopic passivation effect. Furthermore, transient optoelectronic measurements (TCSPC, TPV, and TPC) demonstrate that TMU treatment decisively extends carrier lifetimes and facilitates swift charge extraction. Through this multidimensional investigation, we establish that TMU's optimal coordination chemistry not only unlocks the macroscopic thermodynamic limit but also achieves a record-high power conversion efficiency together with exceptional operational stability.

To systematically tailor the crystallization kinetics of tin perovskite films, we established a solvent library classified into four distinct categories: urea derivatives, common aprotic sulfoxides/amides, cyclic ester-based solvents, and volatile solvents.[4,6] The chemical structures of the twelve selected fuming agents are presented in Figure 1a, this study systematically correlates the inherent physical properties of these solvents with

Received: May 16, 2026
Accepted: June 1, 2026
Published: June 16, 2026

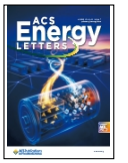

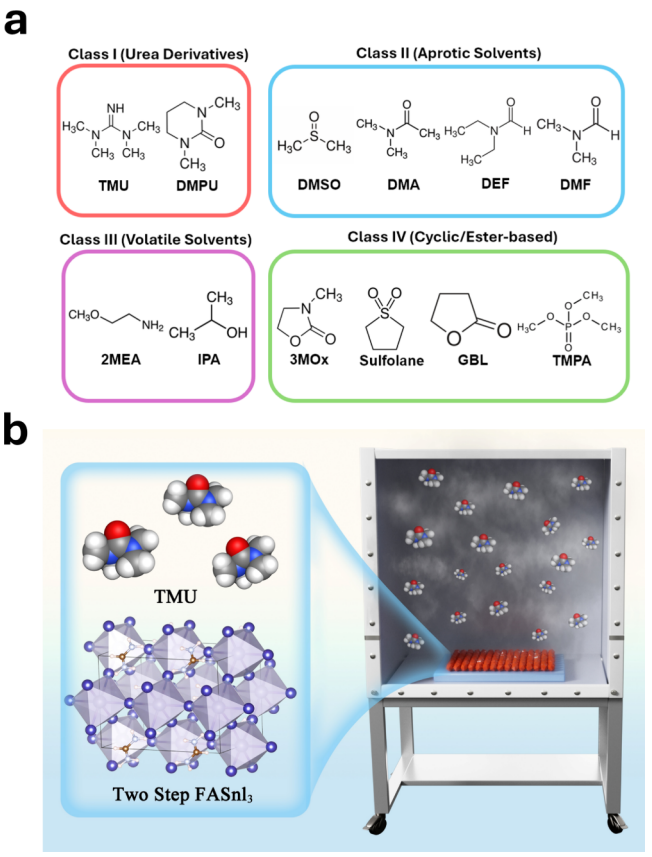

Figure 1. Comparison of twelve SVT solvents and their impact on device performance. (a) Structure of the twelve solvents used for vapor treatment. (b) Solvent vapor treatment.

the final photovoltaic performance of the devices. The fabrication process employs an SVT as illustrated in Figure 1b. We adopt this terminology to emphasize active chemical intervention, where solvent vapors in the glovebox environment interact with the as-crystallized perovskite films to induce a controlled dissolution-recrystallization process. This post-treatment effectively facilitates grain coarsening and defect healing by mobilizing surface ions, distinct from the passive thermal relaxation typically associated with conventional thermal annealing.[7,8]

Among the candidates, 1,1,3,3-tetramethylurea (TMU) emerged as the superior modulator, significantly outperforming the conventional DMSO. While both solvents possess high Gutmann donor numbers (DN ≈ 30) indicative of strong Lewis basicity towards Sn^{2+}, TMU is distinguished by its moderate dielectric constant (ε_r = 24.5) and balanced vapor pressure. This specific physicochemical combination allows TMU to form a stable yet reversible intermediate complex, facilitating a controlled retardation of the crystallization rate. Unlike DMSO, which often induces rapid and disordered nucleation due to its high polarity,[9] the TMU treatment effectively extends the crystal growth window.[10] This regulation promotes the formation of a dense, monolithic morphology with significantly enlarged grains and minimized defect densities, laying the foundation for high-efficiency devices.

To elucidate the molecular-level interactions governing the SVT process, density functional theory (DFT) calculations were performed as a primary screening step to evaluate the adsorption behavior of the twelve solvents on the perovskite surface. As visualized in Figures 2a and S1, the structural optimization reveals the coordination geometries of the fuming agents, where the calculated adsorption energies (ΔE_{ads}) dictate the thermodynamic stability of the solvent-perovskite intermediate complexes (Figure 2b).[11] The calculated ΔE_{ads} values range widely, allowing us to screen the solvents based on their coordination strength. Solvents that interact only weakly with the perovskite surface, like 3MOx (−0.13 eV) and sulfolane (−0.15 eV), lead to insufficient surface passivation and consequently poor device performance. In contrast, TMU (−1.16 eV), alongside traditional fuming agents like DMSO (−0.76 eV) and DMF (−1.38 eV), exhibits a highly favorable adsorption affinity. This demonstrates that TMU provides the robust Lewis basicity necessary for effective surface coordination and defect passivation during the initial stage.

Building upon the DFT results, we further screened these strongly coordinating candidates by evaluating their macroscopic physical parameters, specifically dielectric constant (ε_r), Gutmann donor number (DN), and vapor pressure (P_{vap}). To fully decouple the kinetic and thermodynamic factors governing film formation, we correlated the device efficiency with solvents' P_{vap} and DN,[4,6] as shown in Figure 2c. Figure S2 presents the J−V curves measured under both forward and reverse scan directions. The champion TMU-treated device exhibits negligible hysteresis, indicating that the highly crystalline $FASnI_3$ film effectively suppresses trap-mediated migration at the interfaces. To confirm the reproducibility of the solvent vapor treatment, statistical distributions of photovoltaic parameters (PCE, V_{OC}, J_{SC}, and FF) were collected from 15 independent devices for each condition. As shown in Figure S3 and corresponding statistics in Tables S1−S12, the TMU-treated $FASnI_3$ devices exhibit a narrow distribution with a highly reproducible average PCE, culminating in a champion efficiency of 10.45%. While a high DN (>25 kcal mol^{-1}, strong coordination) is a prerequisite for retarding crystallization, it is not the sole determinant factor for high performance. A distinct volcano-shaped dependence on vapor pressure is observed, identifying an optimal kinetic window between 0.5 and 2.0 Torr, where the TMU-treated device peaks at an optimal efficiency of 10.45%. Solvents with excessive volatility (e.g., IPA, 2MEA) lead to rapid, uncontrollable flash crystallization, whereas those with extremely low volatility (e.g., sulfolane, <0.01 Torr) fail to provide sufficient vapor concentration for effective modulation.[12,13] TMU uniquely occupies the sweet spot in this landscape: it combines a strong Lewis basicity (DN ≈ 31.0) comparable to DMSO with a balanced vapor pressure (P_{vap} = 1.6 Torr). This dual advantage enables TMU to facilitate a controlled dissolution-recrystallization process without the over-dissolution or difficult removal issues often associated with other high-DN solvents.[14,15] This structural superiority directly translates into optimized charge extraction, as corroborated by the incident photon-to-electron conversion efficiency (IPCE) spectrum shown in Figure S4, which reveals a broad photo-response enhancement across the visible-to-NIR region.

To uncover the crystallographic origin of the improved film quality, 1D integrated profiles from GIWAXS were extracted along the in-plane and out-of-plane directions (Figures 3a,b and S5). The most prominent crystallographic difference lies in the specific position of the (100) diffraction peaks. The

https://doi.org/10.1021/acsenergylett.6c01505
ACS Energy Lett. 2026, 11, 5211−5217

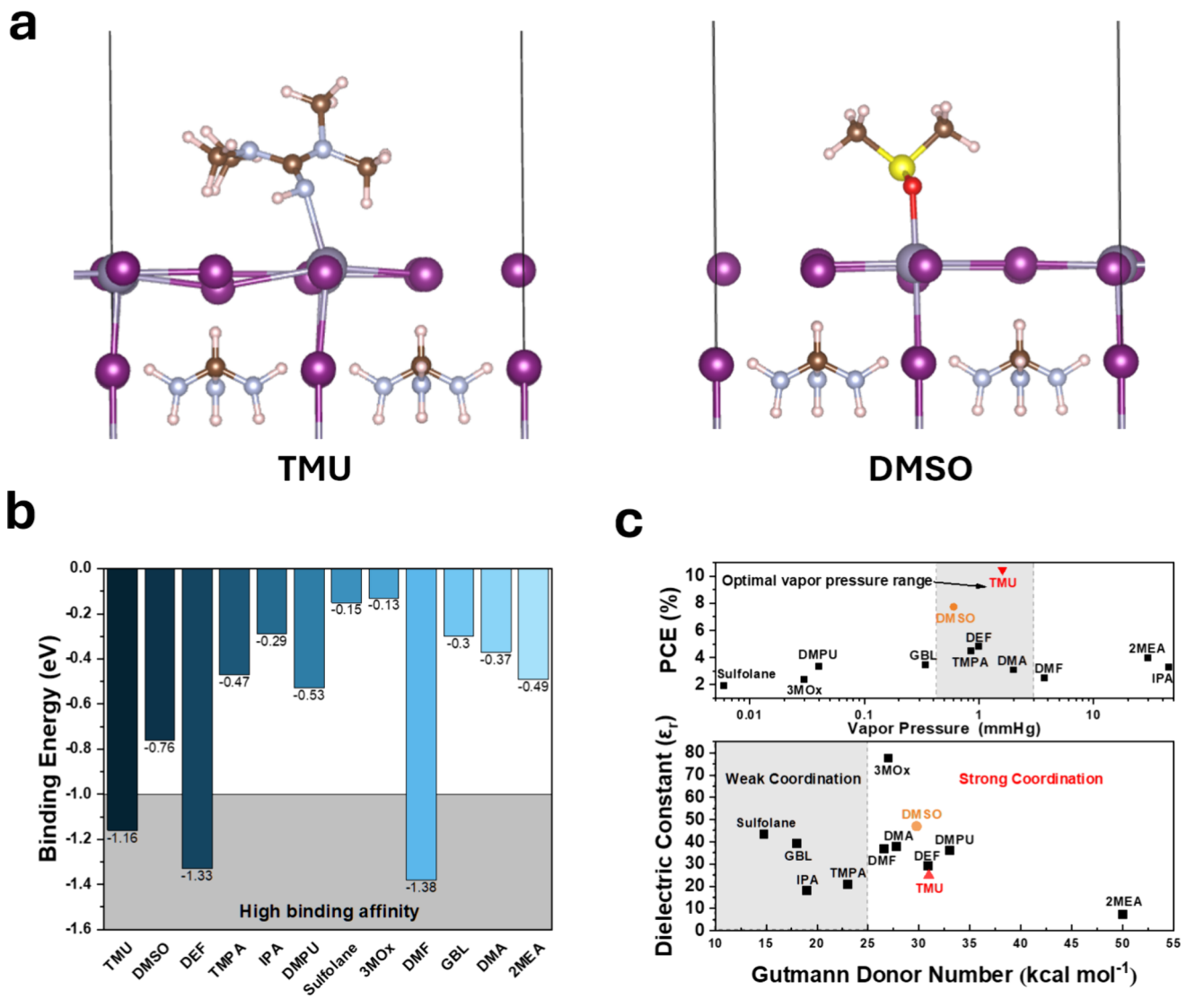

Figure 2. Theoretical and physicochemical characterization of the solvent vapor treatment (SVT) process. (a) DFT-optimized adsorption models of TMU and DMSO on the $FASnI_3$ surface. (b) The adsorption energies (E_{ads}) of the SVT solvent. (c) Physical properties of the SVT solvents.

DMSO-treated film displays a noticeable peak shift towards lower q values $\left(q{\approx}0.99\ \text{Å}^{-1}\right)$. According to the scattering relationship $q = 2\pi/d$, this shift corresponds to a measurable expansion in the crystallographic d-spacing, which is symptomatic of severe residual tensile strain. Such macroscopic lattice expansion is primarily induced by the entrapment of strongly coordinating solvent molecules within the perovskite lattice or at grain boundaries during the rapid crystallization process. In contrast, the TMU-treated film exhibits a distinct peak shift towards higher q values $\left(q{\approx}1.01\ \text{Å}^{-1}\right)$, indicating a well-contracted and highly relaxed lattice.[16] This structural strain analysis directly verifies our previous DFT predictions: TMU's optimal binding affinity provides necessary crystallization modulation but avoids detrimental molecular retention, thereby successfully relieving the residual strain in the final perovskite film.

The thermodynamic potential and spatial distribution of non-radiative recombination were evaluated via QFLS mapping (Figures 3c,d and S6). The film treated with DMSO—the conventional but suboptimal baseline—yields a limited QFLS value of 0.99 eV. While the DMSO map is marred by significant spatial heterogeneity and trap-induced light domains, these severe recombination centers are fundamentally linked to DMSO's inherent physical defects, including the previously discussed residual lattice strain and Sn^{4+} oxidation. In stark contrast, TMU treatment transcends these physical barriers, demonstrating a significantly higher QFLS peaking at 1.028 eV. The exceptionally deep and near-perfectly homogeneous contrast across the entire TMU map demonstrates a transcending macroscopic passivation effect.[17] This comparison definitively proves that while DMSO serves as a standard baseline, its inherent physical shortcomings prevent it from reaching the thermodynamic limit, whereas the strain-free and highly ordered lattice facilitated by TMU successfully maximizes the device's open-circuit voltage (V_{OC}).

The impact of this optimized solvent environment on microstructural evolution is quantified in Figures 3e and S7. Statistical analysis of grain sizes derived from SEM imagery reveals that

https://doi.org/10.1021/acsenergylett.6c01505
ACS Energy Lett. 2026, 11, 5211−5217

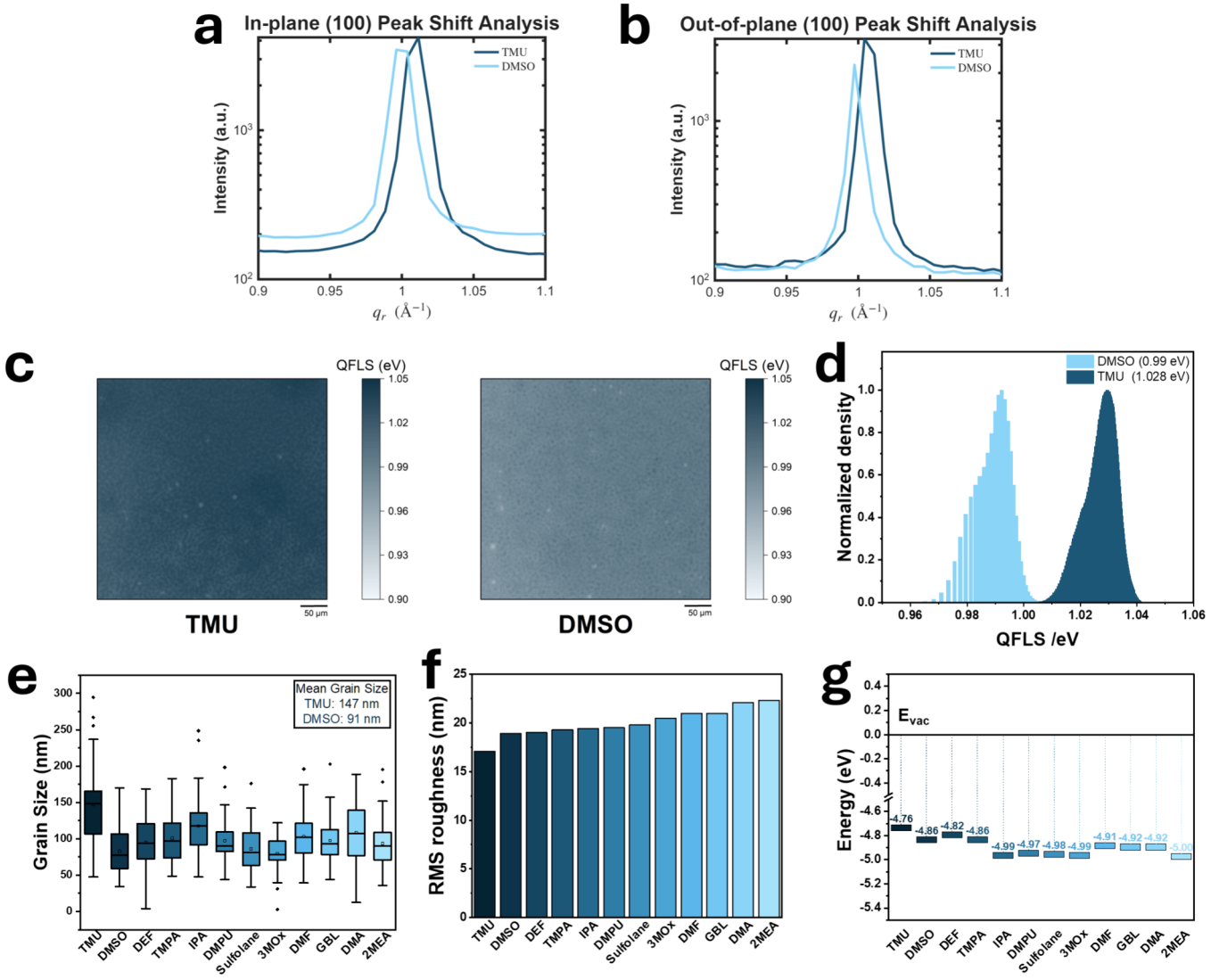

Figure 3. Characterization of tin-based perovskite films treated with twelve different solvent vapor treatment (SVT) processes. (a) In-plane and (b) out-of-plane GIWAXS peak shift analysis for TMU- and DMSO-treated films. (c) QFLS maps and (d) corresponding normalized density distributions. (e) Statistical grain size distribution derived from SEM. (f) Surface roughness (RMS) obtained from AFM. (g) Fermi level (E_F) positions relative to the vacuum level determined by KPFM

the TMU-treated film achieves the largest average grain size of 147 nm, a significant enhancement (~1.6-fold) over the DMSO solvent (grain size ~91 nm). This substantial grain coarsening confirms that the synergistic combination of strong coordination and balanced vapor pressure effectively suppresses nucleation density and promotes monolithic domain growth.

The roughness of the tin-based perovskite films treated with various solvents was characterized by AFM in Figures 3f and S8. Among the twelve solvents investigated, the TMU-treated film exhibited the most superior surface smoothness, with an ultralow roughness of 17.0 nm. In contrast, films treated with solvents such as 2MEA (RMS = 37.8 nm) showed significantly higher roughness. This exceptional flatness indicates that TMU effectively manipulates the crystallization kinetics of the tin-based perovskite, yielding a dense and continuous film. This smooth surface ensures excellent physical contact with the subsequent electron transport layer, thereby minimizing non-radiative recombination at the interface and contributing to the great device performance (PCE 10.45%).[18,19]

To further elucidate the impact of SVT on the perovskite surface, Kelvin Probe Force Microscopy (KPFM) was performed. In Figures 2d and S9, The TMU-treated sample displayed the highest contact potential difference (V_{CPD} = 0.237 V), which corresponds to the lowest surface work function (Φ approx. 4.76 eV) relative to the vacuum level. The extracted V_{CPD} and work function values for the films treated with all twelve investigated solvents are systematically summarized in Table S13. The significant upward shift of the Fermi level (E_F) in the TMU group indicates a substantial reduction in p-type self-doping.[20] This electronic optimization suggests that TMU treatment effectively passivates surface defect states and suppresses the oxidation of Sn^{2+} to Sn^{4+}. The improved film quality is further corroborated by optical characterization. This improved energy band alignment and surface chemical stability are

https://doi.org/10.1021/acsenergylett.6c01505
ACS Energy Lett. 2026, 11, 5211−5217

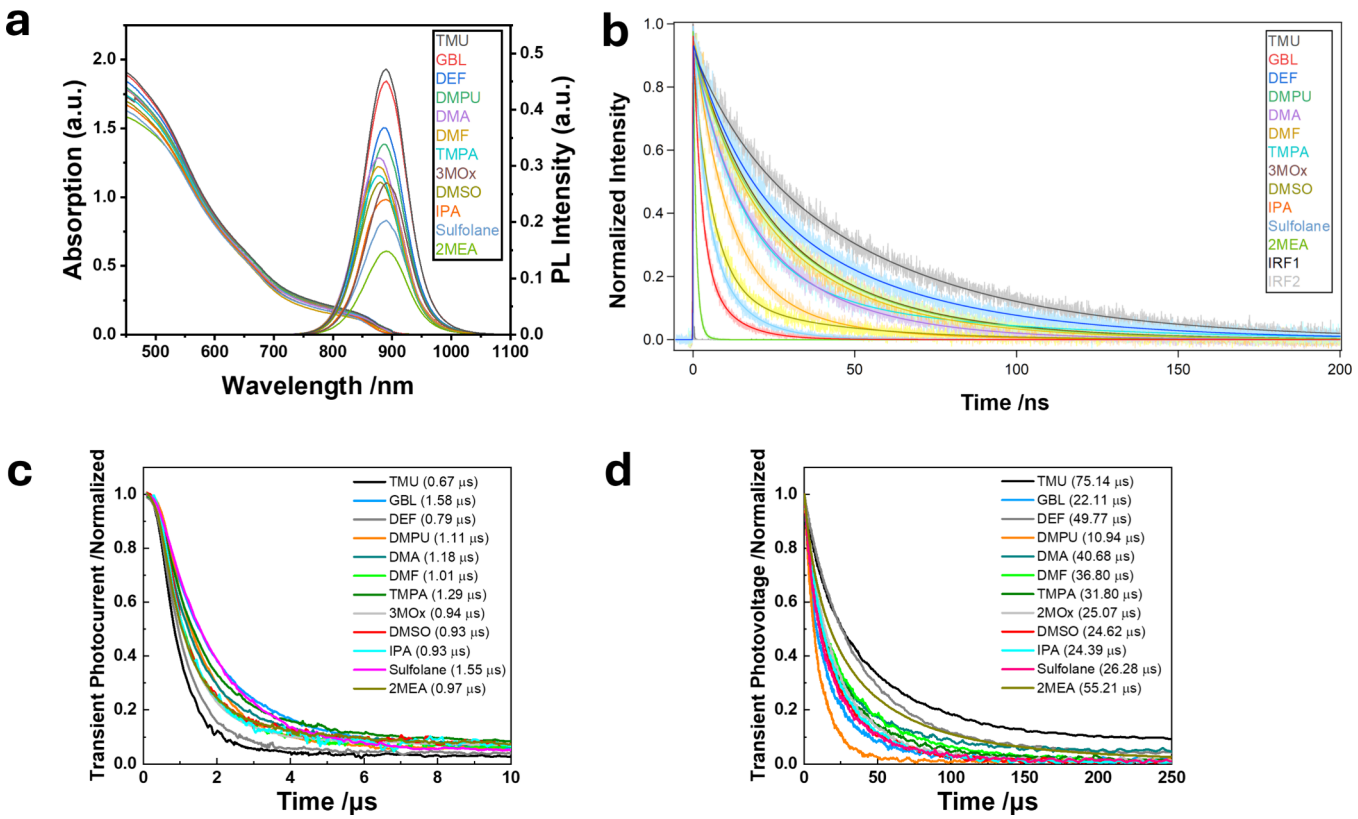

Figure 4. Optoelectronic properties and charge carrier dynamics. (a) Steady-state UV-vis absorption and photoluminescence (PL) spectra of the perovskite films treated with various solvents (PL excitation wavelength: λ_{ex} = 450 nm). (b) Time-resolved PL (TCSPC) decay curves of the corresponding films (excitation wavelength: λ_{ex} = 635 nm, repetition rate: 25 MHz, power: 4 μJ cm^{-2}; detection wavelength: λ_{em} = 840 nm). (c) Transient photocurrent (TPC) and (d) transient photovoltage (TPV) decay profiles of the corresponding devices.

consistent with a remarkable long-term stability exceeding 6000 h in Figure S10, having a much improvement from DMSO. Furthermore, the robust operational stability was confirmed by maximum power point tracking (MPPT) in Figure S11, where the device maintained over 90% of its initial power output after 7 h of continuous operation, highlighting its resistance to light-induced stress.

The photophysical properties of the perovskite films were investigated to evaluate the impact of the solvent treatments (Figure 4a,b). As shown in the UV−Vis spectra, the TMU-treated film exhibits a remarkably sharp absorption onset at approximately 910 nm. This well-defined band-edge feature signifies a significant reduction in energetic disorders and sub-gap tail states. Furthermore, its steady-state photoluminescence (PL) intensity demonstrates a dramatic enhancement over the DMSO benchmark. This pronounced luminescence reflects a maximized radiative-to-non-radiative recombination ratio, suggesting the effective suppression of deep-level trap states.

To quantitatively resolve the recombination kinetics, time-correlated single photon counting (TCSPC) was performed to monitor the transient PL decay profiles of the perovskite films. As depicted in Figure 4b and corresponding fitting in Table S14, the decay behaviors vary significantly depending on the fuming solvent. Notably, the TMU-treated film yields a substantially prolonged average carrier lifetime (τ_{avg}) of 50.8 ns. This remarkable carrier longevity represents a nearly fifty-fold improvement over the DMPU control (1.47 ns),[21] and it also significantly outperforms the conventional DMSO baseline. A longer carrier lifetime generally indicates a higher quality perovskite lattice with fewer non-radiative recombination centers. Consequently, the photo-generated carriers in the TMU-treated film can survive for a much longer duration before recombining, allowing for more efficient charge transport and collection at the respective interfaces. This prolonged carrier extraction window directly contributes to the enhanced open-circuit voltage (V_{OC}) and the superior overall photovoltaic performance of the TMU-based devices.

The charge carrier transport and recombination dynamics in the full devices were investigated using transient photocurrent and photovoltage decay profiles (Figure 4c,d). TPC is associated with the carrier extraction process while TPV profiles characterize carrier recombination process.[22] The TPC profiles in Figure 4c were fitting using mono-exponential function with the corresponding carrier lifetimes marked in the figure. Accordingly, TMU-treated sample exhibits the shortest carrier lifetime, resulting from quick carrier transport between adjacent layers in the device, conducive to yield the best device performance. On the other hand, we fitted the TPV profiles in Figure 4d using bi-exponential functions, whose fitting coefficients are summarized in Table S15. Accordingly, TMU-treated samples exhibit the longest average carrier lifetime, attributed to superior characteristics against undesirable carrier recombination, which is consistent with our TCSPC data.

In conclusion, we have clarified the kinetic and thermodynamic driving forces governing the crystallization of tin perovskites through a systematic solvent vapor treatment study. We

https://doi.org/10.1021/acsenergylett.6c01505
ACS Energy Lett. 2026, 11, 5211−5217

pinpoint a critical "sweet spot" in solvent properties where high Lewis basicity meets moderate vapor pressure, with TMU emerging as the ideal modulator. This specific balance effectively mitigates the rapid, disordered crystallization typical of Sn-based systems, promoting grain coarsening, strain relaxation and defect healing via a controlled dissolution-recrystallization mechanism. Consequently, the optimized films exhibit superior surface quality with ultralow roughness (RMS 17.0 nm) and a favorable energetic landscape, characterized by a minimized work function and reduced p-type self-doping. These microstructural and electronic improvements culminate in a record PCE of 10.45% for the TMU device with robust operational durability and exceptional storage stability exceeding 6000 h. Beyond the specific success of TMU, this research establishes a comprehensive framework for solvent selection, highlighting that environmental control via precise physicochemical matching is a key to unlocking the full potential of lead-free perovskite photovoltaics.

■ ASSOCIATED CONTENT

Supporting Information

The Supporting Information is available free of charge at https://pubs.acs.org/doi/10.1021/acsenergylett.6c01505.

Experimental details, materials, and methods, DFT result, IV result, statistical distribution, IPCE result, GIWAXS results, QFLS results, QFLS results, AFM results, photovoltaic parameters, work functioncalculations, and TCSPC fittingparameters (DOCX)

■ AUTHOR INFORMATION

Corresponding Author

Eric Wei-Guang Diau – *Department of Applied Chemistry and Institute of Molecular Science, National Yang Ming Chiao Tung University, 1001 Ta-Hseuh Rd., Hsinchu 300093, Taiwan; Center for Emergent Functional Matter Science, National Yang Ming Chiao Tung University, 1001 University Road, Hsinchu 30010, Taiwan;* orcid.org/0000-0001-6113-5679; E-mail: diau@nycu.edu.tw

Authors

Che-Hsin Kuo – *Department of Applied Chemistry and Institute of Molecular Science, National Yang Ming Chiao Tung University, 1001 Ta-Hseuh Rd., Hsinchu 300093, Taiwan*

Yun-Sheng Shih – *Department of Applied Chemistry and Institute of Molecular Science, National Yang Ming Chiao Tung University, 1001 Ta-Hseuh Rd., Hsinchu 300093, Taiwan*

Chun-Hsiao Kuan – *Department of Applied Chemistry and Institute of Molecular Science, National Yang Ming Chiao Tung University, 1001 Ta-Hseuh Rd., Hsinchu 300093, Taiwan; Center for Emergent Functional Matter Science, National Yang Ming Chiao Tung University, 1001 University Road, Hsinchu 30010, Taiwan*

Shi-Jie Shen – *Department of Applied Chemistry and Institute of Molecular Science, National Yang Ming Chiao Tung University, 1001 Ta-Hseuh Rd., Hsinchu 300093, Taiwan*

Yi-Hao Wu – *Department of Applied Chemistry and Institute of Molecular Science, National Yang Ming Chiao Tung University, 1001 Ta-Hseuh Rd., Hsinchu 300093, Taiwan*

Hsin-Yu Hu – *Department of Applied Chemistry and Institute of Molecular Science, National Yang Ming Chiao Tung University, 1001 Ta-Hseuh Rd., Hsinchu 300093, Taiwan*

Han-Jung Li – *Department of Chemistry, Chung Yuan Christian University, Chungli District, Taoyuan City 320314, Taiwan;* orcid.org/0009-0003-7749-5558

Chieh-Ting Lin – *Department of Chemical Engineering, National Chung Hsing University, Taichung 40227, Taiwan; Innovation and Development Center of Sustainable Agriculture, National Chung Hsing University, Taichung 40227, Taiwan;* orcid.org/0000-0002-9591-0888

Complete contact information is available at: https://pubs.acs.org/doi/10.1021/acsenergylett.6c01505

Author Contributions

‡C.-H.K., Y.-S.S., and C.-H.K. equally contributed to this work.

Notes

The authors declare no competing financial interest.

■ ACKNOWLEDGEMENTS

The authors thank Ms. Y.-T. Lee and Prof. C.-S. Lin with the FEG-SEM experiments at the Instrumentation Center of National Taiwan University. The authors appreciated Ms. Y.-T. Liao and Prof. T.-J. Yen of NTHU Instrumentation center for the AFM/KPFM measurements. The authors express our gratitude for the assistance with GIWAXS data analysis given by Drs. Y.-W. Tsai and J.-M. Lin at TPS 25A1, NSRRC. This work was supported by the National Science and Technology Council (NSTC), Taiwan (grant nos. NSTC 112-2636-M-009-006, NSTC 113-2639-M-A49-001-ASP, and NSTC 114-2639-M-A49-001-ASP), and by the Center for Emergent Functional Matter Science, National Yang Ming Chiao Tung University (NYCU), through the Featured Areas Research Center Program within the Higher Education Sprout Project of the Ministry of Education (MOE), Taiwan.

■ REFERENCE

(1) Stoumpos, C. C.; Kanatzidis, M. G. The renaissance of halide perovskites and their evolution as emerging semiconductors. *Acc. Chem. Res.* **2015**, *48* (10), 2791–2802.

(2) Hao, F.; Stoumpos, C. C.; Guo, P.; Zhou, N.; Marks, T. J.; Chang, R. P. H.; Kanatzidis, M. G. Solvent-Mediated Crystallization of $CH_3NH_3SnI_3$Films for Heterojunction Depleted Perovskite Solar Cells. *J. Am. Chem. Soc.* **2015**, *137* (35), 11445–11452.

(3) Song, T.-B.; Yokoyama, T.; Stoumpos, C. C.; Logsdon, J.; Cao, D. H.; Wasielewski, M. R.; Aramaki, S.; Kanatzidis, M. G. Importance of reducing vapor atmosphere in the fabrication of tin-based perovskite solar cells. *J. Am. Chem. Soc.* **2017**, *139* (2), 836–842.

(4) Hamill, J. C.; Schwartz, J.; Loo, Y.-L. Influence of Solvent Coordination on Hybrid Organic–Inorganic Perovskite Formation. *ACS Energy Lett.* **2018**, *3* (1), 92–97.

(5) Shahbazi, S.; Li, M.-Y.; Fathi, A.; Diau, E. W.-G. Realizing a cosolvent system for stable tin-based perovskite solar cells using a two-step deposition approach. *ACS Energy Lett.* **2020**, *5* (8), 2508–2511.

(6) Marcus, Y. *The properties of solvents*; Wiley, **1998**.

(7) Zhao, X.; Liu, T.; Kaplan, A. B.; Yao, C.; Loo, Y.-L. Accessing Highly Oriented Two-Dimensional Perovskite Films via Solvent-Vapor Annealing for Efficient and Stable Solar Cells. *Nano Lett.* **2020**, *20* (12), 8880–8889.

(8) Liao, H.-C.; Tsao, C.-S.; Huang, Y.-C.; Jao, M.-H.; Tien, K.-Y.; Chuang, C.-M.; Chen, C.-Y.; Su, C.-J.; Jeng, U.-S.; Chen, Y.-F.

Insights into solvent vapor annealing on the performance of bulk heterojunction solar cells by a quantitative nanomorphology study. *RSC Adv.* **2014**, *4* (12), 6246–6253.
(9) Hao, F.; Stoumpos, C. C.; Cao, D. H.; Chang, R. P. H.; Kanatzidis, M. G. Lead-free solid-state organic–inorganic halide perovskite solar cells. *Nat. Photonics* **2014**, *8* (6), 489–494.
(10) Zhu, H.; Zhong, Y.; You, J.; Jiang, Z.; He, X.; Xu, C.; Dai, Z.; Xu, G.; Song, Q. Tetramethylurea Based Intermediate Phase Engineering for Efficient and Stable Perovskite Solar Cells. *Small* **2025**, *21* (17), 2412717.
(11) Huang, S.-H.; Tian, K.-Y.; Huang, H.-C.; Li, C.-F.; Chu, W.-C.; Lee, K.-M.; Huang, Y.-C.; Su, W.-F. Controlling the morphology and interface of the perovskite layer for scalable high-efficiency solar cells fabricated using green solvents and blade coating in an ambient environment. *ACS Appl. Mater.* **2020**, *12* (23), 26041–26049.
(12) Xiao, Z.; Dong, Q.; Bi, C.; Shao, Y.; Yuan, Y.; Huang, J. Solvent annealing of perovskite-induced crystal growth for photovoltaic-device efficiency enhancement. *Adv. Mater.* **2014**, *26* (37), 6503–6509.
(13) Luo, P.; Xia, W.; Zhou, S.; Sun, L.; Cheng, J.; Xu, C.; Lu, Y. Solvent engineering for ambient-air-processed, phase-stable $CsPbI_3$ in perovskite solar cells. *J. Phys. Chem. Lett.* **2016**, *7* (18), 3603–3608.
(14) Lee, S. J.; Shin, S. S.; Kim, Y. C.; Kim, D.; Ahn, T. K.; Noh, J. H.; Seo, J.; Seok, S. I. Fabrication of efficient formamidinium tin iodide perovskite solar cells through SnF_2–pyrazine complex. *J. Am. Chem. Soc.* **2016**, *138* (12), 3974–3977.
(15) Yokoyama, T.; Cao, D. H.; Stoumpos, C. C.; Song, T.-B.; Sato, Y.; Aramaki, S.; Kanatzidis, M. G. Overcoming short-circuit in lead-free $CH_3NH_3SnI_3$ perovskite solar cells via kinetically controlled gas–solid reaction film fabrication process. *J. Phys. Chem. Lett.* **2016**, *7* (5), 776–782.
(16) Wu, J.; Liu, S.-C.; Li, Z.; Wang, S.; Xue, D.-J.; Lin, Y.; Hu, J.-S. Strain in perovskite solar cells: origins, impacts and regulation. *Natl. Sci. Rev.* **2021**, *8* (8), nwab047.
(17) El-Hajje, G.; Momblona, C.; Gil-Escrig, L.; Ávila, J.; Guillemot, T.; Guillemoles, J.-F.; Sessolo, M.; Bolink, H. J.; Lombez, L. Quantification of spatial inhomogeneity in perovskite solar cells by hyperspectral luminescence imaging. *Energy Environ. Sci.* **2016**, *9* (7), 2286–2294.
(18) Shao, Y.; Xiao, Z.; Bi, C.; Yuan, Y.; Huang, J. Origin and elimination of photocurrent hysteresis by fullerene passivation in $CH_3NH_3PbI_3$ planar heterojunction solar cells. *Nat. Commun.* **2014**, *5* (1), 5784.
(19) Lin, R.; Xiao, K.; Qin, Z.; Han, Q.; Zhang, C.; Wei, M.; Saidaminov, M. I.; Gao, Y.; Xu, J.; Xiao, M. Monolithic all-perovskite tandem solar cells with 24.8% efficiency exploiting comproportionation to suppress Sn(ii) oxidation in precursor ink. *Nat. Energy* **2019**, *4* (10), 864–873.
(20) Shao, S.; Liu, J.; Portale, G.; Fang, H. H.; Blake, G. R.; ten Brink, G. H.; Koster, L. J. A.; Loi, M. A. Highly reproducible Sn-based hybrid perovskite solar cells with 9% efficiency. *Adv. Energy Mater.* **2018**, *8* (4), 1702019.
(21) Herz, L. M. Charge-carrier dynamics in organic-inorganic metal halide perovskites. *Annu. Rev. Phys. Chem.* **2016**, *67* (1), 65–89.
(22) Kasparavičius, E.; Franckevičius, M.; Driukas, S.; Gulbinas, V. Charge carrier dynamics at the perovskite interface with self-assembled monolayers. *ACS Appl. Mater. Interfaces* **2024**, *16* (43), 59477–59487.

https://doi.org/10.1021/acsenergylett.6c01505
ACS Energy Lett. 2026, 11, 5211–5217